The Response of a He−3 Fermi Liquid Droplet to Vibronic Excitation of an Embedded Glyoxal Molecule

ARTICLE *in* THE JOURNAL OF PHYSICAL CHEMISTRY A · JUNE 2014

Impact Factor: 2.69 · DOI: 10.1021/jp503184d · Source: PubMed

3 AUTHORS:

Giorgio Benedek
Università degli Studi di Milano-Bicocca
321 PUBLICATIONS **3,765** CITATIONS
SEE PROFILE

Vladimir Hizhnyakov
University of Tartu
190 PUBLICATIONS **1,620** CITATIONS
SEE PROFILE

Peter Toennies
Max Planck Institute for Dynamics and Self-…
724 PUBLICATIONS **20,759** CITATIONS
SEE PROFILE

THE JOURNAL OF PHYSICAL CHEMISTRY A

Article

pubs.acs.org/JPCA

The Response of a ^{3}He Fermi Liquid Droplet to Vibronic Excitation of an Embedded Glyoxal Molecule

Giorgio Benedek,[†,‡,§] Vladimir Hizhnyakov,[∥] and J. Peter Toennies*[,§]

[†]Donostia International Physics Center (DIPC), University of the Basque Country (EHU-UPV), Paseo de Lardizàbal 4, 20018 Donostia/San Sebastian, Spain

[‡]Dipartimento di Scienza dei Materiali, Università di Milano-Bicocca, Via Cozzi 53, 20125 Milano, Italy

[§]Max-Planck Institut für Dynamik und Selbstorganisation, Am Fassberg 17, 37077 Göttingen, Germany

[∥]Institute of Physics, University of Tartu, Riia tu. 142, 202400 Tartu, Estonia

ABSTRACT: The zero-phonon line (ZPL) and the sideband in the vibronic spectrum of a single glyoxal molecule inside a ^{3}He droplet are analyzed within the framework of the Lax formalism. The new theory takes full account of the coupling of the molecule to the single particle−hole (PH) and collective excitations of the doped Fermionic droplet. The effect on the coupling of the wavevector dependence of the effective ^{3}He mass and the large local density of the first ^{3}He shell, resulting from the interaction with the chromophore, are also included in the theory. By fitting of a coupling parameter and the phase factor between the PH and collective response functions, the shape and relative intensity of the observed ZPL and its slowly decreasing multiexcitation sideband are well-reproduced. The new theory is consistent with the previous explanation of the surprisingly sharp phonon line superimposed on the sideband in terms of the dense first ^{3}He shell, which acts as a Helmholtz resonator for the zero sound of the droplet.

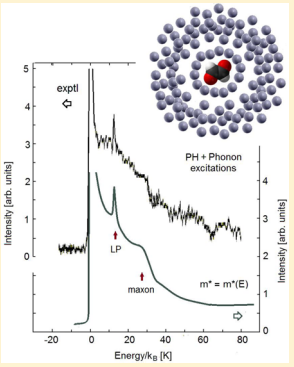

1. INTRODUCTION

The spectroscopy of single molecules embedded inside large helium droplets ($N \approx 10^3$−10^4 atoms) provides a new fascinating probe of the elementary excitations of quantum fluids.[1−4] Inside bosonic ^{4}He droplets, the vibronic absorption spectrum of a molecule exhibits in addition to a sharp zero-phonon line (ZPL) a rich satellite structure that often bears information about the elementary excitations of the surrounding quantum liquid.[1,2,5−7] In the case of the $S_1 \leftarrow S_0$ electronic transition of the glyoxal molecule ($C_2H_2O_2$) and several other molecules in ^{4}He droplets, a distinct pseudogap on the blue side of the ZPL separates it from a well-defined satellite phonon-wing-like peak with an energy of E_{PW} = 0.69 meV (=5.6 cm^{-1} = 8.1 K).[5,8] The energy of the phonon wing agrees with the increased density of states at excitations of the ^{4}He superfluid (Figure 1a).[9] This observation provided the first direct evidence for the superfluidity of ^{4}He droplets.

The present article addresses the interpretation of the vibronic spectra of glyoxal in Fermionic ^{3}He droplets of about the same size as the ^{4}He droplets ($N \approx 10^3$−10^4 atoms).[10,11] The corresponding experiments were carried out in order to confirm the interpretation of the roton peak in ^{4}He droplets and to date are the only available measurements of vibronic spectra of a molecule in ^{3}He.[10] Instead of the pseudogap and adjacent roton peak on the blue side of the ZPL, the ZPL is followed by an attached long, slowly decreasing tail with an unexpected superimposed sharp peak at E_{LP} = 0.99 meV (=8.05 cm^{-1} = 11.5 K).[10] In the following, this peak will be called a localized phonon (LP) peak. The marked difference in the sideband structure compared with that of ^{4}He droplets provided confirmation for the interpretation of the ^{4}He droplet spectrum as giving direct evidence for the superfluidity of ^{4}He droplets.

In a previous theoretical study, the slowly decreasing tail was attributed entirely to the continuum spectrum of Fermi liquid particle−hole (PH) excitations.[12,13] As shown in Figure 1b, in a Fermi liquid (FL) the density of states of particle−hole excitations in the low-energy limit is large, and the contribution of these excitations to the spectrum of an embedded molecule becomes nonperturbatively strong. The present theory shows that as a result the ZPL acquires a finite, albeit small, width even at zero temperature, with a strongly asymmetric shape and without a pseudogap between the ZPL and the sideband. In a previous theoretical investigation,[10] the superimposed LP peak and its exceptional sharpness, with a full width at half-maximum (fwhm) 15 times smaller than that for the bulk phonon peak measured by neutron scattering in the bulk at the same energy,[12−14] was shown to be due to localized vibrations associated with the Friedel-like ^{3}He liquid density buildup surrounding the chromophore molecule.

The aim of the present article is to provide a more complete theoretical description of the observed sideband in ^{3}He droplets that takes into account, in addition to PH and local-

Special Issue: Franco Gianturco Festschrift

Received: March 31, 2014
Revised: June 4, 2014

   dx.doi.org/10.1021/jp503184d | J. Phys. Chem. A XXXX, XXX, XXX−XXX

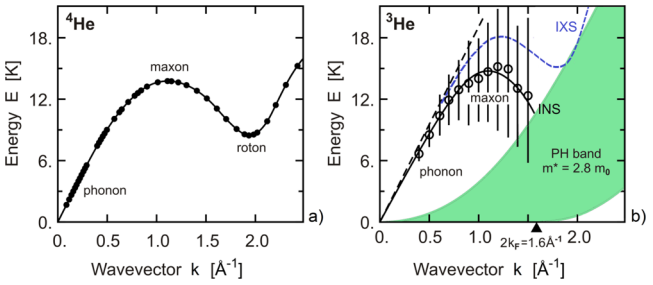

Figure 1. Comparison of the elementary excitations in bulk liquid ^{4}He[9] and ^{3}He.[12−14] Whereas the phonon branches of the two quantum liquids are quite similar, ^{3}He has in addition a broad particle−hole (PH) band (shadowed area) that extends upward from the lowest energies,[13,14] here represented for the case of a constant ^{3}He effective mass $m^* = 2.8m_0$ corresponding to its value at the Fermi level, where $k_F = 0.8$ Å^{-1} is the Fermi wavevector and m_0 is the free-atom mass. The decay of phonons into single and multiple PH excitations explains the large full width at half-maximum (fwhm) of the phonon lines (vertical bars) observed with inelastic neutron scattering (INS) at 0.12 K.[13] The inelastic X-ray scattering (IXS) data at 1.10 K (dashed line, interpolating the data from ref 14) also show an apparent roton minimum in a region where, however, collective excitations are gradually converted into PH excitations for increasing momentum. As shown in Figure 2e, the PH band for the realistic case of a wavevector-dependent effective mass actually covers the phonon branch beyond the maxon wavevector, thus accounting for phonon−PH mixing and the large fwhm in that region.

mode excitations, the effects of the coupling of the optical transitions to the collective phonon excitations in doped ^{3}He droplets. As in our previous investigations,[10,11] we use the time-dependent Lax formalism.[15] In the previous publications,[10,11] the comparatively long sideband tail of the 0_0^0 absorption line was attributed to multiple PH excitations on the basis of an empirical convolution of the single PH spectrum. However, since the PH and collective phonon excitations of the FL are inextricably connected in their density−density response function,[16] they need to be treated on an equal basis. The present theory takes into account the effect of the ^{3}He liquid density buildup surrounding the chromophore molecule on the PH excitations. In a second step, the coupling between the PH and phonon excitations is taken into account via their convolution and the relative phase shift to obtain the combined excitation spectrum. The resulting simulation provides an excellent description of the entire spectrum, including the sharp localized phonon, with only a single adjusted coupling strength parameter and an assumed phase shift.

The Lax theory used here was first introduced to deal with optically excited impurities in solids at low temperatures, where it is well-established that the ZPL observed in the weak-coupling regime is accompanied by a sideband due to phonon-assisted transitions.[17]

2. BASIC EQUATIONS

2.1. The Lax Theory. The Lax equation for the Fourier transform of the spectral function $I(\mathcal{E})$ of an optical center in condensed matter reads as[15]

$$F(t) = \langle e^{itH_2} e^{-itH_1} \rangle \tag{1}$$

where $\langle ... \rangle$ denotes a quantum-statistical average, H_1 and H_2 are the Hamiltonians of the doped ^{3}He droplet in the initial (ground) and final (excited) electronic states of the molecule, respectively, and $\hbar$ has been set equal to 1 (in eq 1 and hereafter). Throughout this article, $\mathcal{E}$ is used to denote an energy transfer. As shown previously,[10] the shape of a ZPL and its low-energy sideband caused by the dynamics of the surrounding FL receive a major contribution from the continuum of PH excitations. As in classical solids and also in liquid ^{4}He, the collective phonon excitations contribute much less to the low-energy ZPL part of the spectrum. Thus, the spectral features of particle−hole excitations are analyzed first, while the role of the collective phonon excitations are discussed later on (section 4), as their contribution is necessary for a quantitative account of the experimental sideband.

To describe the optical spectrum by means of the Lax approach,[15] we perform the standard canonical transformation to quasi-particles (q-particles) and quasi-holes (q-holes) (e.g., see ref 18). Then for pure particle−hole excitations H_1 and H_2 are written in the following manner, which frequently is called the Hartree approximation:[18]

$$H_1 = \sum_i (\varepsilon_{pi} \hat{a}_i^+ \hat{a}_i + \varepsilon_{hi} \hat{b}_i^+ \hat{b}_i) \tag{2}$$

$$H_2 = H_1 + V_q \tag{3}$$

in which

$$V_q \equiv \sum_{ij} V_{ij} (\hat{a}_i^+ \hat{a}_j + \hat{a}_i^+ \hat{b}_{-j}^+ + \hat{b}_{-i} \hat{a}_j + \hat{b}_{-i} \hat{b}_{-j}^+) \tag{4}$$

where $\hat{a}_i^+$ and $\hat{a}_i$ are the creation and annihilation operators, respectively, for a q-particle of energy $\varepsilon_{pi} = E_i - E_F \equiv \varepsilon_i$ *above* the Fermi level (E_F) and $\hat{b}_{-i}^+$ and $\hat{b}_{-i}$ are the creation and annihilation operators, respectively, for a q-hole of energy $\varepsilon_{hi} = E_F - E_i = -\varepsilon_i$ *below* the Fermi level. Since the annihilation operator of a particle with energy $E_i < E_F$ is equivalent to the creation operator of the corresponding hole with energy $\varepsilon_{hi} = E_F - E_i$, both of the energies ε_{pi} and ε_{hi} are defined to be positive. Spin indices are omitted since the coupling of the ^{3}He spin degrees of freedom to the electronic transition of the molecule is negligibly small. In eq 4, V_{ij} is the matrix element between a q-particle state and a q-hole state of the interaction potential that couples the dipole-active electronic transition of the molecule to the nearby helium atoms. Four possible transitions are taken into account in eq 4: two across the Fermi level ($\hat{a}_i^+ \hat{b}_{-j}^+, \hat{b}_{-i} \hat{a}_j$) and two either above ($\hat{a}_i^+ \hat{a}_j^+$) or below ($\hat{b}_{-i} \hat{b}_{-j}$) the Fermi level. For an explicit evaluation of V_q as defined by eq 4, it should be noted that the smallest energy of q-particles due to finite-size quantization is on the order of $V^{-2/3}\hbar^2/m^*$, where m^* is the ^{3}He effective atomic mass and V is the droplet volume.[19] For droplets with $N \approx 5 \times 10^3$ atoms, this energy is in the μeV range. Since it is much smaller than the experimental spectral resolution of the measurements reported in ref 10, the effects of size quantization can be neglected, and the sums over wavenumbers can be replaced by integrals over the respective energies.

In eqs 2 and 4 the indices $i \equiv (k, l, m)$ and $j \equiv (k', l', m')$ group the quantum numbers of q-particles and q-holes in the spherical potential provided by the droplet, where l and m are the angular momentum quantum numbers and k is the radial momentum quantum number. As mentioned above, spin indices are omitted since the coupling of ^{3}He spin degrees of freedom to the electronic transition of the molecule is negligibly small. Here spin fluctuations contribute only to the wavevector dependence of the effective mass near the Fermi level. As in the case of usual metals, we take the same effective

dx.doi.org/10.1021/jp503184d | J. Phys. Chem. A XXXX, XXX, XXX−XXX

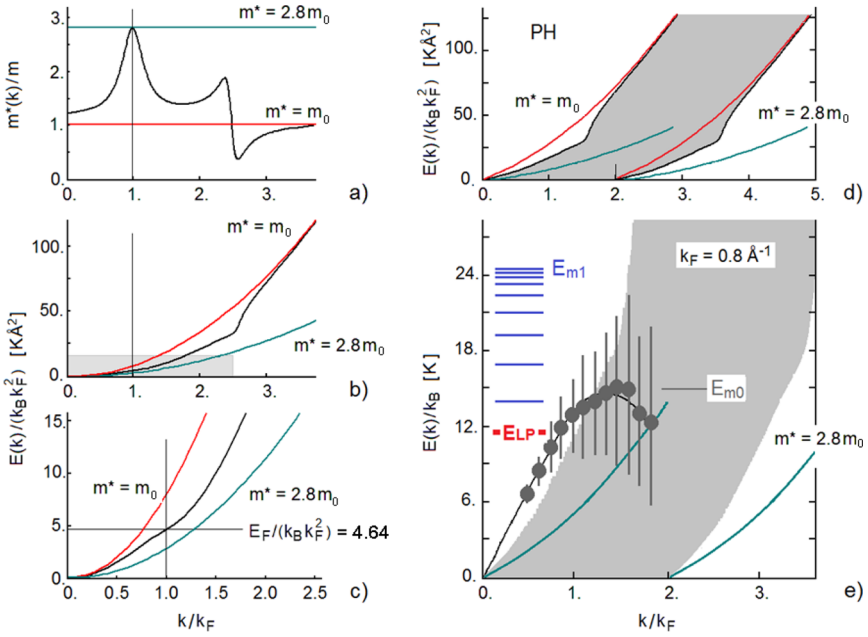

Figure 2. (a) Effective mass $m^*(k)$ of ^{3}He in the homogeneous liquid phase in units of the free-atom mass m_0 as a function of the wavevector k relative to the Fermi wavevector k_F (black curve), from data first reported by Friman and Krotschek.[20] The peak at the Fermi wavevector k_F and the oscillation at about $2.4k_F$ are attributed to the combined effects of mass- and spin-density fluctuations.[20,23] (b) Comparison of the dispersion relation corresponding to (a) obtained by integration of the inverse effective mass (black curve) with the dispersion relations for a constant effective mass $m^* = 2.8m_0$ corresponding to the effective mass at the Fermi level m_F^* (blue curve) and for $m^* = m_0$ (red curve). The single-particle dispersion curves inside the shadowed area are shown on a larger scale in (c). (d) PH excitation spectral band (gray area) for the momentum-dependent effective mass. The edges of the spectrum tend to the free-particle dispersion curves. (e) Experimental collective excitation (phonon) branch (● and solid line) with the corresponding widths for the bulk FL[12,13] superimposed on the low-momentum and low-energy part of the PH spectrum for $k_F = k_{F0} = 0.8$ Å^{-1} and momentum-dependent effective mass. The large Landau broadening as the phonon branch overlaps with the PH spectrum should be noted. The blue horizontal bars qualitatively represent the radial phonon spectrum of the first shell, including the totally symmetric localized phonon (LP) breathing mode of energy E_{LP} (red line).

mass m^* chosen for q-particles and q-holes near the Fermi surface.[16]

2.2. Effect of the First Shell on the Matrix Elements. In the present theory, in contrast to ref 10, we account for the effect on the matrix elements resulting from the buildup in density of the first shell of ^{3}He atoms surrounding the chromophore. To quantify this effect, it is first necessary to consider the momentum dependence of the effective mass $m^*(k)$ of the ^{3}He atoms. As shown first by Friman and Krotscheck[20] and confirmed by more recent theories,[21−23] $m^*(k)$, the effective mass of ^{3}He atoms in the liquid phase, is increased at the bulk Fermi wavevector k_{F0} by a factor of 2.8 with respect to the free particle mass and in addition exhibits a large oscillation at around sk_{F0} with $s \approx 2.4$[23] (Figure 2a). Such deviations arise from the coupling of the q-particle motion with density and spin fluctuations.[23] In particular, the oscillation at sk_{F0} is associated with the maximum in the frequency (maxon) of collective phonon modes, which for the bulk liquid is at $E_{m0} \approx 15$ K (Figure 2e).[12,13] From the definition of the momentum-dependent effective mass as $m^*(k) \equiv k[\partial E(k)/\partial k]^{-1}$, where $E(k)$ is the q-particle energy band,[21−23] and an analytical fit of $m^*(k)$[24] (Figure 2a), numerical integration of $k/m^*(k)$ yields the dispersion relation $E(k)$ (Figure 2b,c) in agreement with that reported by Fåk and Glyde in the vicinity of k_{F0}.[21] For the bulk ^{3}He density ($\rho_0 = 0.017$ Å^{-3}) and its Fermi wavevector ($k_{F0} = 0.8$ Å^{-1}), this gives $E_{F0} \equiv E(k_{F0}) = 2.97$ K for a momentum-dependent effective mass.

The use of the correct wavevector dependence of m^* and of the corresponding nonparabolic dispersion $E(k)$ has significant effects. This can be readily appreciated from Figure 2b,c by comparing the latter with the parabolic dispersion curves for constant (k-independent) effective masses $m^* = m_0$, where m_0 is the mass of the free ^{3}He atom, and $m^* = 2.8m_0 \equiv m_F^*$, the effective mass of atoms at the Fermi level. This is the value currently used to describe the ^{3}He atom in the bulk liquid. In what follows, it is convenient to consider m^* as a function of energy, $m^*(k(E)) \equiv m^*(E)$, via the inverse dispersion relation $k(E)$.

As a result of the interaction of the chromophore with the surrounding helium, the density within the first shell around the central molecule is much larger than that in the undisturbed bulk, ρ_0; the density of the unperturbed liquid under standard conditions, which is about the same as the density in large droplets, is $\rho_0 = 0.017$ Å^{-3}.[25] As shown in ref 26, in the case of SF_6 the density in the first shell has a *peak* value as large as 0.076 Å^{-3}, with an *average* value $\overline{\rho}_1$ of about $2\rho_0$. Since glyoxal and SF_6 have comparable electronic polarizabilities (4.71 Å^3[27] and 4.49 Å^3,[28] respectively) and their orientation-averaged van der Waals potential well depths are not too different (41 K[29] and 63 K,[30] respectively) we assume that the SF_6 densities apply to glyoxal. It should be noted that at the droplet temperature the glyoxal is essentially in its rotational ground state, as the lowest rotational excitation energy of the free molecule is above 1 K. In a local density approximation, the corresponding Fermi wavevector can be estimated from the simple expression $k_{F1} = (\overline{\rho}_1/\rho_0)^{1/3}k_{F0}$,[16] which yields $k_{F1} = 1.01$ Å^{-1}; also, according to Figure 2c, $E_{F1} \equiv E(k_{F1}) = 4.71$ K. This is a significant increase relative to the bulk liquid, for which $k_{F0} = 0.8$ Å^{-1} and $E_{F0} \equiv E(k_{F0}) = 2.97$ K. The maxon energy E_{m1} for the internal modes of the first shell for the average shell density

dx.doi.org/10.1021/jp503184d | J. Phys. Chem. A XXXX, XXX, XXX−XXX

$\overline{\rho}_1 \approx 2\rho_0 = 0.034$ Å^{-3} can then be estimated from the energy at the wavevector $2.4k_{F1}$, which from Figure 2b,c is $E(sk_{F1}) = 29$ K. As will be shown later (see section 4.2), this result is consistent with the observation of a shoulder in the phonon part of the sideband. It should be noted that at the larger average first-shell density ($k_{F1} = 1.01$ Å^{-1}), the Fermi energy for a constant effective mass $m^* = 2.8m_0$ would have been only $E_{F1} = 2.85$ K (Figure 2c), which is about that for the bulk liquid but variable effective mass.

The assumption of a scaling that provides $m^*(E)$ and the maxon energy at any density in terms of the corresponding k_F value and the factor s is a key feature of the model. The maxon energy explicitly depends on the local average density $\overline{\rho}_1$, so the latter could be determined from the position of the experimental feature associated with the maxon. However, this dependence is rather weak because of the cube root linking $\overline{\rho}_1$ to k_{F1}, so determining $\overline{\rho}_1$ from the experimental maxon energy can be as uncertain as choosing the calculated value for SF_6, and the latter approach has been preferred. To give an idea, for $\overline{\rho}_1$ varying from $1.5\rho_0$ to $3\rho_0$, the corresponding E_{m1} varies from 24 to 38 K. The experimental value of 29 K indicates that $\overline{\rho}_1$ for glyoxal cannot be very different from that calculated for SF_6.

The following qualitative arguments also suggest that $k_{F1} = 1.01$ Å^{-1} is a reasonable choice for the first solvation shell around glyoxal. As illustrated in Figure 3, the integrated first-shell density peak[25] contains about 16 atoms, with an average interatomic distance that is estimated to be reduced from 3.9 Å in the bulk to 3.7 Å. This alone implies for a repulsive potential a steep r^{-12} stiffening of the local force constants as large as about 70%. The additional interaction with the glyoxal molecule yields a further increase in the force constants felt by the atoms of the first shell, leading, as argued above, to a first-shell localized elementary excitation maxon energy E_{m1} that is considerably larger than the maxon energy for the unperturbed undoped liquid.

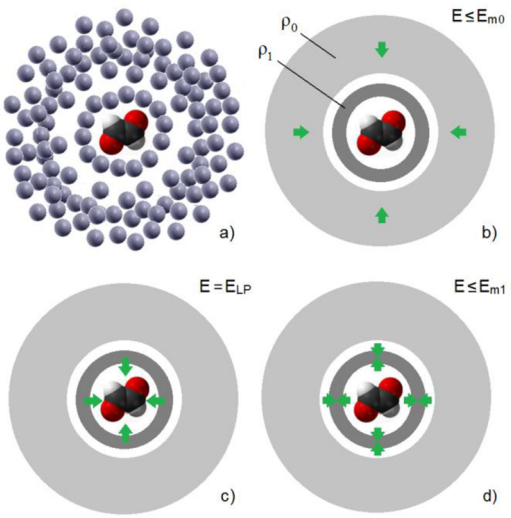

Figure 3. (a) Representation of a ^{3}He liquid droplet showing a dense first shell (snowball) around a glyoxal molecule. The spectrum of collective radial excitations of the doped droplet is schematically split into three components: (b) the quasi-continuum spectrum of bulk modes similar to that of the undoped liquid, with a maximum (maxon) energy E_{m0}; (c) a radial localized phonon (LP) resonance of the first shell as a whole (all atoms of the shell move radially in phase) with energy E_{LP}; and (d) the quasi-continuum spectrum of the radial shell internal modes with a maxon energy E_{m1}.

It is important to realize that the first shell is not at all isotropic and that the effective mass is in fact a tensor with a radial component $m^*_\perp$ and two equal tangential components $m^*_\parallel$. In a homogeneous FL the effective mass increases with density[31] to the extent that an extrapolation to a density equal to $\overline{\rho}_1$ for an isotropic liquid would actually yield a solid with a diverging m^*.[32] Thus, despite the large radial density, the atoms in the first shell preserve their mobility in the radial direction, whereas the compression (or even crystallization, i.e., localization) within the thin crust of the first shell determining a large peak density hinders tangential motions of the atoms, with $m^*_\parallel$ eventually diverging. Since, as discussed below, only radial collective excitations are involved, hereafter the momentum-dependent effective mass $m^*(k)$ shall be identified with $m^*_\perp$ and taken to be the same as for the undoped droplet, the only effect of the larger shell density being the corresponding increase in k_F. From here on the index 1 (or 0) labeling the Fermi wavevector and energy of the first shell (or the bulk) shall be omitted in equations that hold in both cases.

The increased density in the first shell affects the interaction potential that couples the dipole-active electronic transition of the molecule to the helium atom positions. The electronic wave functions of the molecule, and therefore the electronic transition energy, depend on the ^{3}He atom positions via the overlap with the wave functions of the He atoms. Such dependence can then be derived from their orthogonality conditions.[33] As shown by the density functional theory calculations of Barranco and co-workers[25,26] for a SF_6 molecule at the center of a ^{3}He droplet, the overlap between the molecular orbitals and the He orbitals becomes appreciable at a distance of at least 4 Å away from the center of the SF_6 molecule and about 2.5 Å away from the peripheral atoms of the molecule (SF bond length ≈ 1.56 Å). In glyoxal the conditions are expected to be similar. Thus, it is argued that only the spherical components of the molecule orbitals with the largest extension, that is, those with the lowest angular quantum numbers l give some contribution. Since in ^{3}He the infrared spectra indicate that the molecular rotations are completely damped and the orientation of the molecule is nearly entirely random,[34,35] it can be assumed that in the electronic transition ($l = l'$, $m = m'$) no angular momentum is transferred to the FL and moreover that only the spherical ($l = 0$) FL excitations couple to the electronic transition, which means that $V_{ij} \rightarrow V_{k00,k'00}$. Thus, the matrix elements are independent of the shape of the molecule, which greatly simplifies the following discussion.

In ref 10, the radial parts of the molecule ground- and excited-state wave functions were assumed to decay exponentially with the distance r from the center as $\exp(-\kappa_g r)$ and $\exp(-\kappa_e r)$, respectively. The matrix element of the potential $V_{k00,k'00}$ is proportional to the inelastic part of the transition-dipole matrix element calculated in ref 10 (see eq 7 therein) via a proportionality constant f_1/e, where e is the electron charge and f_1 is the force exerted by the electronic transition on the atoms of the first shell:

$$V_{k00,k'00} = 6\left(\frac{4}{3}\right)^9 f_1(\overline{\rho}_1 a_0^3)\frac{(\kappa_e\kappa_g)^{3/2}}{(\kappa_e + \kappa_g - iQ)^4} \quad (5)$$

where a_0 is the Bohr radius and $Q \equiv k' - k$. The force f_1 depends on the shell radius R_1 as $\exp(-2\kappa R_1)$, where $\kappa = (\kappa_g +$

dx.doi.org/10.1021/jp503184d | J. Phys. Chem. A XXXX, XXX, XXX−XXX

$\kappa_e)/2$ is on the order of one atomic unit. In the following we assume that $\kappa_g = \kappa_e = \kappa \equiv a_0^{-1}$. In principle, eq 5 applies to any further shell of radius R_n and density ρ_n with the replacement of $f_1\rho_1$ by $f_n\rho_n$; however, the force decays quite rapidly with distance, and therefore, only the force acting on the first shell is considered here.

In dealing with the momentum transfer Q that appears in eq 5, it is convenient to consider the limits of Q to be much smaller or much larger than any Fermi wavevector k_F. At these limits, Q is directly related to the single particle−hole excitation energy $\mathcal{E}$ as $Q \approx \mathcal{E}m_F^*/k_F$ and $Q \approx (2m\mathcal{E})^{1/2}$, respectively (with $\hbar = 1$).[36] With the above asymptotic expressions, Q in eq 5 can now be expressed as a function of the energy transfer, where the crossover from the low- to the high-energy regime is located at $E_{co} = 2mk_F^2/(m_F^*)^2$:

$$|V_{k00,k'00}|^2 \approx \frac{V_0^2}{(1 + Q^2/4\kappa^2)^4} = \begin{cases} V_0^2\left[1 + \left(\frac{m_F^*\mathcal{E}}{2k_F\kappa}\right)^2\right]^{-4} & \mathcal{E} < E_{co} \\ V_0^2\left[1 + \frac{m\mathcal{E}}{(4\kappa)^2}\right]^{-4} & \mathcal{E} \geq E_{co} \end{cases} \equiv V_0^2\varsigma(\mathcal{E}) \quad (6)$$

where $V_0 \equiv 2(4/3)^8 f_1\rho_1 a_0^3(\kappa_g\kappa_e)^{3/2}/\kappa^4 \approx 20 f_1\rho_1 a_0^4$.

3. FOURIER TRANSFORM

3.1. Fourier Transform of the Spectral Function. To calculate the Fourier transform of the spectral function (eq 1), in the Dirac interaction picture (with $\hbar = 1$) we write the following:[37]

$$\exp[it(H_1 + V_q)] = \hat{T}\exp\left[\int_0^t d\tau\, V_q(\tau)\right]\exp[itH_1] \quad (7)$$

where $\hat{T}$ is the time-ordering operator and $V_q(t) = e^{itH_1}V_q e^{-itH_1}$. This makes it possible to apply the cumulant expansion to eq 1:

$$F(t) = \exp\left[i\langle V_q\rangle t + \sum_{n=2}^{\infty} g_n(t)\right] \quad (8)$$

where

$$g_n(t) = \frac{i^n}{n!}\int_0^t dt_1 \int_0^t dt_2 \cdots \int_0^t dt_n\, \langle \hat{T}V_q(t_1)V_q(t_2)\cdots V_q(t_n)\rangle_c \quad (9)$$

and the subscript c means that only closed diagrams are taken into account. The number of cumulants needed increases with the strength of the interaction. In the case under consideration, the interaction is rather weak, and the main contribution is given by the second cumulant. This allows one to use the approximation

$$F(t) \approx \exp\left[i\langle V_q\rangle t - \int_0^t dt_1 \int_0^{t_1} dt_2\, \langle \hat{V}_q(t_1)\hat{V}_q(t_2)\rangle\right] \quad (10)$$

where $\hat{V}_q = V_q - \langle V_q\rangle$. The time-dependent perturbation, despite its weakness, causes nonperturbatively strong effects at low energy, which does not allow one to work with $F(t)$ at only short times and to replace the exponential with its linear expansion.

3.2. Correlation Function of Fermi Quasi-Particles. The fact that any potential−potential correlation function, such as that appearing in eq 10, is associated with a *response function* $\varphi(\mathcal{E})$ via a Fourier transform,

$$\varphi(\mathcal{E}) \equiv \frac{1}{2\pi}\int_{-\infty}^{\infty} dt\, e^{-i\mathcal{E}t}\langle \hat{V}_q(t)\hat{V}_q(0)\rangle \quad (11)$$

allows the integrations over t_2 and t_1 in eq 10 to be readily performed. Thus, the Fourier transform of the spectral function takes the form

$$F(t) = \exp[it\delta + g_2(t)] \quad (12)$$

where

$$\delta = \langle V_q\rangle - \int_{-\infty}^{\infty} d\mathcal{E}\, \frac{\varphi(\mathcal{E})}{\mathcal{E}} \quad (13)$$

determines the shift of the ZPL due to the surrounding droplet with respect to the ZPL energy of the free molecule. The two terms on the right-hand side of eq 13 are the static and dynamic contributions. The second-order cumulant

$$g_2(t) = \int_{-\infty}^{\infty} d\mathcal{E}\, \frac{\varphi(\mathcal{E})}{\mathcal{E}^2}(e^{it\mathcal{E}} - 1) \quad (14)$$

provides, via its Fourier transform, the shape of sideband spectral intensity $I(\mathcal{E})$.[38]

The potential−potential correlation function contains all of the information on the PH dynamics and, once the interatomic interaction is switched on, also on the collective phonon dynamics (see section 4.2). For PH excitations, the double sum over all initial and final states in the momentum space is conveniently transformed into a double integral over the initial- and final-state energies. By means of eqs 4, 7, and 8 with the assumption of constant and equal q-hole and q-particle effective masses, the potential−potential correlation function takes on the comparatively simple form

$$\langle \hat{V}_q(t)\hat{V}_q(0)\rangle = \alpha \iint d\varepsilon d\varepsilon'\, \{\varsigma(\varepsilon - \varepsilon')[\overline{p}_\varepsilon(1 - \overline{p}_{\varepsilon'})e^{-it(\varepsilon-\varepsilon')} + (1 - \overline{h}_\varepsilon)\overline{h}_{\varepsilon'}e^{it(\varepsilon-\varepsilon')}] + \varsigma(\varepsilon + \varepsilon')[\overline{p}_\varepsilon\overline{h}_{\varepsilon'}e^{-it(\varepsilon+\varepsilon')} + (1 - \overline{h}_\varepsilon)(1 - \overline{p}_{\varepsilon'})e^{it(\varepsilon+\varepsilon')}]\} \quad (15)$$

where $\overline{p}_k$ and $\overline{h}_k$ are the Fermi occupation numbers of q-particles and q-holes, respectively. The prefactor α on the right-hand side is given by $\alpha \equiv V_0^2E_F/E_{co}^3$ and provides a dimensionless measure of the coupling strength. All of the occupation numbers refer to the ^{3}He droplet temperature of $T = 0.15$ K[10] (however, see refs 34 and 35). In eq 15, the first two terms in the curly brackets represent the simultaneous creation of a q-particle and a q-hole, while the last two terms represent the simultaneous creation of a quasiparticle (q-particle or q-hole) and annihilation of another quasiparticle of the same type. For each term in eq 15, the sums are restricted to values of k and k' for which the q-particles and q-holes have positive energies (i.e., $\varepsilon_{p,k00}$, $\varepsilon_{p,k'00}$, $\varepsilon_{h,k00}$, $\varepsilon_{h,k'00} > 0$). It should be noted that in eq 15, if the effects of size quantization are neglected, it is possible to replace the sums over the discrete cluster states k and k' by integrals over the energies $\varepsilon \equiv kk_F/m^*$ and $\varepsilon' \equiv k'k_F/m^*$, respectively.

For the explicit evaluation of the PH contribution $\varphi_{PH}(\mathcal{E})$ to the total $\varphi(\mathcal{E})$, we note that the energy of annihilated q-

dx.doi.org/10.1021/jp503184d | J. Phys. Chem. A XXXX, XXX, XXX−XXX

particles ε' is smaller than k_BT, which is in turn much smaller than the cutoff energies E_F and E_{co}, and therefore, $\varsigma(\varepsilon + \varepsilon') \approx \varsigma(\varepsilon - \varepsilon')$. Thus, for a positive energy $\mathcal{E}$, after the occupation numbers in eq 15 are replaced with their temperature-dependent expressions, we explicitly obtain the response function $\varphi_{PH}(\mathcal{E})$ as

$$\varphi_{PH}(\mathcal{E}) = \alpha\varsigma(\mathcal{E}) \int_0^\infty \frac{d\varepsilon}{(1 + e^{-\beta\varepsilon})(1 + e^{\beta(\varepsilon-\mathcal{E})})} \times [1 - \Theta(\varepsilon - E_F)\Theta(\mathcal{E} - \varepsilon) + \Theta(\varepsilon - \mathcal{E})\Theta(E_F - \varepsilon)] \quad (16)$$

where $\beta = 1/k_BT$. Using the identity

$$\frac{1}{(1 + e^{-\beta\varepsilon})(1 + e^{\beta(\varepsilon-\mathcal{E})})} = \frac{1}{e^{\beta\varepsilon} - 1}\left(\frac{1}{e^{-\beta\varepsilon} + e^{-\beta\mathcal{E}}} - \frac{1}{1 + e^{-\beta\varepsilon}}\right) \quad (17)$$

allows the integral in eq 16 to be calculated analytically with respect to the variable $z = e^{-\beta\varepsilon}$ to give

$$\varphi_{PH}(\mathcal{E}) = \frac{\alpha\varsigma(\mathcal{E})}{1 - e^{-\beta\mathcal{E}}}\left[\mathcal{E} + \beta^{-1} \ln \frac{1 + e^{-\beta E_F}}{1 + e^{\beta(\mathcal{E}-E_F)}}\right] \quad (18)$$

The PH response function is $\varphi_{PH}(\mathcal{E}) \approx \alpha k_BT$ for $\mathcal{E} \ll k_BT$ and therefore tends to a constant finite value for $\mathcal{E} \to 0$. Thus, no pseudogap between the ZPL and the PH sideband is expected. In the case of variable effective mass, eq 18 still holds approximately provided that the prefactor $\varsigma(\mathcal{E})$ is replaced by

$$\varsigma^*(\mathcal{E}) = \varsigma(\mathcal{E}) \int_0^{E_F} d\varepsilon \left(\frac{4\varepsilon}{9E_F^3}\right)^{1/2} \frac{m^*(\mathcal{E} + \varepsilon)}{m_F^*} \quad (19)$$

The correction factor originates from the mass-dependent Jacobian implied in the conversion of momentum-space integration into an integration over energy and provides an acceptable approximation for $\mathcal{E} > E_F$.

As discussed in section 4.2 a pseudogap occurs if only the phonon sideband is considered. This is because the phonon response function for $\mathcal{E} \to 0$ is proportional to $\alpha\mathcal{E}^n(k_BT/\mathcal{E}) = \alpha\mathcal{E}^{n-1}k_BT$, where $n = 2$ for a three-dimensional bulk and $n = 4$ for localized phonons of even ($l = 0$) symmetry,[39] as in the present case.

4. SPECTRAL SHAPE

4.1. PH Excitations Alone. In the following, the above theory is applied to the analysis of the absorption spectrum of a glyoxal molecule inside a ^{3}He droplet.[10] The shape of the sideband spectral intensity for PH excitations is obtained from the Fourier transform of $F(t)$ (eq 12) by first neglecting the ZPL shift δ. Inserting eq 18 into eq 14, one obtains

$$I(\mathcal{E}) = \int_{-\infty}^{+\infty} dt\, e^{-it\mathcal{E}+g_2(t)} = \int_{-\infty}^{+\infty} dt\, e^{-it\mathcal{E}} \exp\left[\alpha \int_{-\infty}^{\infty} d\varepsilon \frac{e^{i\varepsilon t} - 1}{1 - e^{-\beta\varepsilon}} \frac{\varsigma^*(\varepsilon)}{\varepsilon^2} \times \left(\varepsilon + \beta^{-1} \ln \frac{1 + e^{-\beta E_F}}{1 + e^{\beta(\varepsilon-E_F)}}\right)\right] = e^{-S} \int_{-\infty}^{+\infty} dt\, e^{-it\mathcal{E}} \exp\left[\int_{-\infty}^{\infty} d\varepsilon\, e^{i\varepsilon t} \frac{\varphi_{PH}(\varepsilon)}{\varepsilon^2}\right] \quad (20)$$

where

$$S \equiv \int_{-\infty}^{\infty} d\varepsilon \frac{\varphi_{PH}(\varepsilon)}{\varepsilon^2} \quad (21)$$

is the Huang–Rhys (HR) exponent,[40] which gives the average number of elementary excitations produced by the electronic transition.

Examples of spectra calculated with eq 20 for different values of α, the coupling strength for PH excitations, have been reported in ref 11 for a homogeneous liquid and a constant m^*. In all cases, the transition from the weak- to the strong-coupling regime is signaled by a small shift of the spectral maximum from the ZPL position at $\mathcal{E} = 0$ to increasing positive energy transfer, corresponding to a growing average number of elementary PH excitations. This behavior qualitatively reflects the asymmetric shape of the observed lines (notably the 0_0^0 and 8_0^1 lines[10,11]), as noted in section 2. In the previous analysis,[10] in addition to the continuum of PH excitations only the excitations of the phonons localized in the first ^{3}He shell were considered. These phonon excitations were assumed for simplicity to be those of the uniform liquid and were treated separately on the basis of the argument that their spectra are well-separated in the energy–momentum space. Actually the first-shell PH and collective phonon excitation spectra that couple most strongly to the glyoxal electronic transitions are quite different from those of the uniform liquid as a result of the increase in k_F with the particle density in the first shell adjacent to the chromophore, as discussed in section 2.2. Moreover, adding to $\varphi_{PH}(\mathcal{E})$ the phonon response function, denoted as $\varphi_{phon}(\mathcal{E})$, would lead to a tight entanglement of single-particle and collective excitations via the convolutions implied by eq 20. All that considered, it appears that the simultaneous fit of the sideband shape and the ZPL intensity relative to that of the multiexcitation sideband leads to a much stronger coupling of the electronic transition to collective phonon excitations than to the PH excitations. This is indeed expected for a dense system, although the removal of the pseudogap (or dip) between the ZPL and the sideband is exclusively due to PH excitations. The essential role of the collective phonon excitations in addition to those of the first shell is discussed in the next section.

4.2. The Phonon Contribution. Although the bulk phonon dispersion curve shows some overlap with the PH excitation spectrum (Figure 2 e, momentum-dependent mass case), the phonon response function $\varphi_{phon}(\mathcal{E})$ projected onto the first shell and the PH response function $\varphi_{PH}(\mathcal{E})$ will be treated as *additive*, as done in ref 10, since the main contributions to $\varphi_{phon}(\mathcal{E})$ come from the LP resonance and the other even-symmetry radial modes of the first shell. Because of the comparatively large diameter of the first shell (about 8

dx.doi.org/10.1021/jp503184d | J. Phys. Chem. A XXXX, XXX, XXX–XXX

Å), only bulk modes with a small radial wavevector ($<\pi/8$ Å^{-1}) concur in building up the localized modes, so the coupling of the first-shell phonon modes to PH excitations should be very small at their respective energies, ensuring the *additivity* of their response functions.

The phonon modes of the atomic shells surrounding the glyoxal molecule (C_{2h} point group) that couple to the glyoxal electronic transition have even symmetry (A_g, B_g) with respect to the center of the molecule. Since the breathing (A_g) vibrational mode of the atomic shell involves a modulation of its volume, it is strongly affected by the local increase in the density and force constants. The difference between the bulk and first-shell densities and force constants leads to an impedance mismatch for bulk zero-sound waves, which are therefore scattered by the molecule with no significant response of the shell atoms at any energy, except around the energy at which the force constant and density change effects cancel out, where the shell strongly responds to the incoming bulk wave.[10] Thus, the projected breathing phonon spectrum is just a narrow resonance (the one observed at E_{LP} = 11.5 K) superimposed upon a weak bulk background. This means that the doping molecule dressed by first-shell ^{3}He atoms acts as a resonating cavity in a fluid medium,[41] like a *quantum Helmholtz resonator* for zero sound. Although this resonance frequency lies within the bulk phonon spectrum, it is considered to be a localized phonon (LP) on the basis of its spatial isolation. The calculations by Barranco et al. for a SF_6 dopant[25] show that the first shell contains about 16 atoms. Thus, excluding rigid translations and rotations, the first shell has $3(16) - 6 = 42$ collective degrees of freedom, one-half of them ($\mathcal{N} = 21$) having gerade symmetry: besides the totally symmetric breathing resonance of energy E_{LP}, the first-shell spectrum also includes another 20 internal collective modes of the shell of A_g and B_g symmetry with a frequency spectrum that is considerably stiffer than that of the bulk continuum as a result of the larger density. In particular, the maxon energy of the first shell, E_{m1}, which produces the oscillation in $m^*(k)$ at sk_F, should be about twice E_{m0}.

Using the Lorentzian shape derived in ref 10 for the LP dynamic form factor and a Debye form for the bulk continuum (vanishing as $\mathcal{E}^4$ as required by the projection onto a local totally symmetric coordinate[39]) allows the corresponding phonon response function to be written as

$$\varphi_{\text{phon}}(\mathcal{E}) = \frac{1}{1 - e^{-\beta\mathcal{E}}} \frac{f_1^2 \varsigma(\mathcal{E})}{2|\mathcal{E}|m_F^* \mathcal{N}} \left[\frac{\eta\Gamma_{LP}/\pi}{(|\mathcal{E}| - E_{LP})^2 + \Gamma_{LP}^2} + \frac{5\mathcal{E}^4}{E_{m1}^5}(\mathcal{N} - \eta)c(|\mathcal{E}| - E_{m1}) \right] \tag{22}$$

where $\eta = \rho_0/(\rho_1 - \rho_0)$ is the inverse of the first-shell relative density change, E_{LP} is the LP energy, given by

$$E_{LP} = \frac{1}{\sqrt{2}} E_{m0} - \eta\, \text{Re}(\chi_{11}^0)^{-1} \tag{23}$$

and Γ_{LP} is the LP half-width, given by[10]

$$\Gamma_{LP} = -\eta\, \text{Im}(\chi_{11}^0)^{-1} \tag{24}$$

In eqs 23 and 24, $\chi_{11}^0(\mathcal{E})$ is the projection of the unperturbed (bulk) phonon Green's function onto the first shell,[10,39] and the corresponding unperturbed phonon density is assumed to have a Debye-like form for symmetric modes:

$$\frac{1}{\pi}\, \text{Im}\, \chi_{11}^0(\mathcal{E}) = \frac{5\mathcal{E}^4}{E_{m0}^5} c(|\mathcal{E}| - E_{m0}) \tag{25}$$

where $c(\varepsilon) = 1/(1 + e^{\varepsilon/\Gamma})$ is a cutoff function that sets in beyond the bulk maxon energy E_{m0} and Γ accounts for the phonon line width at the maxon energy.[14] The phonon density of the first-shell internal modes (the second term in the square brackets in eq 22) is also given in a Debye-like form, though with the maxon energy rescaled for the larger first-shell density [$E_{m1} = E(sk_{F1})$] as discussed in section 2.2. Normalization of the total projected phonon density to unity is ensured by the factor of $1/\mathcal{N}$ in eq 22. For $\rho_1 \to \rho_0$, the normalized total phonon density reduces to π^{-1} Im $\chi_{11}^0(\mathcal{E})$ with no resonant feature, as expected.

When projected onto the shell subspace of the atoms surrounding the glyoxal molecule, the PH and phonon parts of the global response function resulting from the sum over the radial component of the wavevector are superimposed, as illustrated in the inset of Figure 4. Thus, the addition of $\varphi_{\text{phon}}(\mathcal{E})$ to $\varphi_{\text{PH}}(\mathcal{E})$ should include a possible phase shift θ between the two competing channels of collective and single PH excitations. Thus, instead of eq 20, the sideband spectral intensity including both PH and phonon contributions should in fact read as follows:

$$\begin{aligned} I(\mathcal{E}) &= \int_{-\infty}^{+\infty} dt\, e^{-it\mathcal{E}+g_2(t)} \\ &= e^{-S} \int_{-\infty}^{+\infty} dt\, e^{-it\mathcal{E}} \\ &\quad \times \exp\left[\int_{-\infty}^{\infty} d\varepsilon\, e^{i\varepsilon t} \frac{\varphi_{\text{PH}}(\varepsilon) + e^{-i\theta\, \text{sgn}(\varepsilon t)} \varphi_{\text{phon}}(\varepsilon)}{\varepsilon^2} \right] \end{aligned} \tag{26}$$

where

$$S \equiv \int_{-\infty}^{\infty} d\varepsilon\, \frac{\varphi_{\text{PH}}(\varepsilon) + \varphi_{\text{phon}}(\varepsilon)}{\varepsilon^2} = S_{\text{PH}} + S_{\text{phon}} \tag{27}$$

is the total HR exponent,[40] which can be expressed as the sum of the HR exponents for PH and phonon excitations. The HR exponent, which is proportional to α, gives the average number of elementary excitations created by the electronic transition; S values greater than 1 conventionally indicate strong coupling. The phase shift θ determines the peculiar characteristic Fano-like shape of the sharp LP resonance superimposed upon the PH continuum. The value $\theta = -\pi/4$ was found to reproduce best the observed shape and has been adopted in Figures 4 and 5.

It is important to remark that the sequence of Fourier transforms in eq 26 produces an entanglement of the two response functions, which means that the PH excitations are coupled with all types of collective excitations (LP, localized, and bulk phonon projections on the first shell). Since they occur in an exponential form, their coupling increases with the order of the convolution, leading to a smearing and smoothening of the tail at higher energy.

4.3. Comparisons with the Experimental Spectrum. Calculations of $I(\mathcal{E})$ for a droplet temperature of 0.15 K with a variable effective mass $m^*(E)$ and a constant effective mass $m^* = m_F^* = 2.8m_0$ are shown in Figures 4 and 5, respectively, where they are compared with the experimental relative depletion spectrum. In all of the calculations, the ZPL maximum was fixed

dx.doi.org/10.1021/jp503184d | J. Phys. Chem. A XXXX, XXX, XXX−XXX

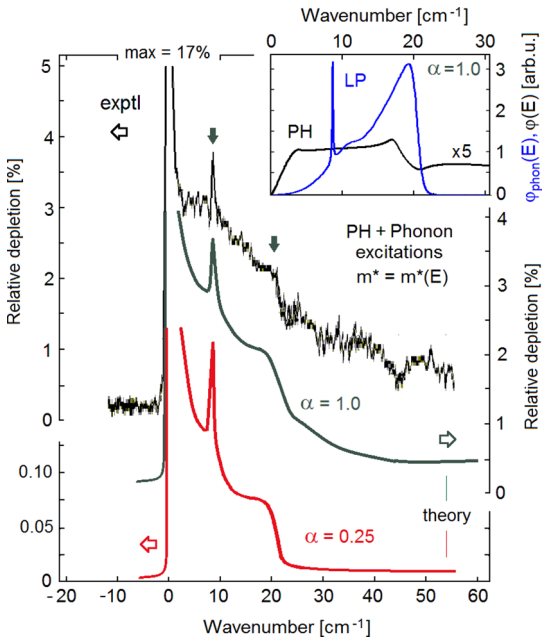

Figure 4. Comparison of the calculated spectrum of the ZPL and its sideband due to both particle–hole (PH) and collective phonon excitations with the experimental spectrum for the 0_0^0 line of glyoxal inside a ^{3}He droplet. The calculations were performed using a variable energy-dependent ^{3}He effective mass $m^*(E)$ and two different values of the coupling strength for PH excitations α.The salient experimental features (marked by vertical arrows) are the sharp LP resonance and the maxon frequency of the first shell, and they are well-reproduced by theory. The value $\alpha = 1$ (strong coupling) correctly reproduces the ratio of the inelastic sideband intensity to the ZPL intensity, whose maximum was fitted to the experimental relative depletion of 17%. The weak-coupling value $\alpha = 0.25$ yields a much weaker inelastic part with respect to the ZPL intensity (also fixed at 17% depletion). The inset compares the shapes and relative intensities of the PH and phonon response functions used in the calculation for $\alpha = 1$. The PH contribution has been multiplied by a factor of 5 for increased visibility. Thus, the glyoxal electronic transition couples to collective phonon excitations much more strongly than to single PH excitations.

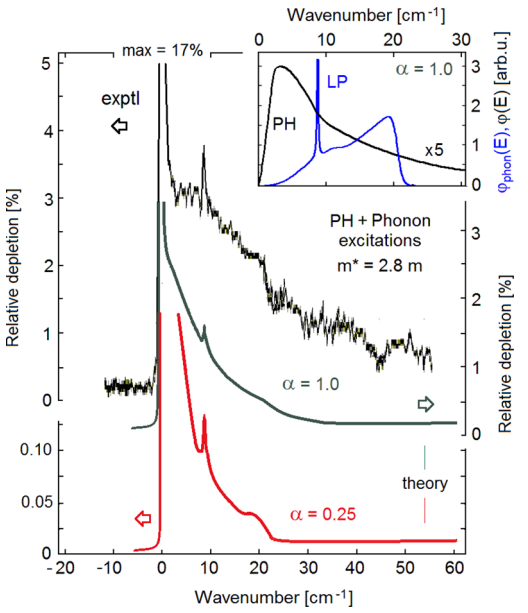

Figure 5. Same as Figure 4 with the same two values of the coupling strength but using a constant ^{3}He effective mass equal to the value at the Fermi level, $m_F^* = 2.8m_0$. Compared with the variable effective mass results shown in Figure 4, the long sideband tail seen in the experiment is not well-reproduced because m^* is not allowed to decrease to the bare mass value m at high energy.

at the experimental value of the depletion (17%). In both Figures 4 and 5 a first-shell maxon linewith of $2\Gamma = 1$ K gave the best fit. For both variable and constant effective mass, the results for two values of α are shown, one in the strong-coupling regime ($\alpha = 1$) and one in the weak-coupling regime ($\alpha = 0.25$). From Figures 4 and 5 it is apparent that the strong-coupling regime ($\alpha = 1$) combined with a variable effective mass provides the best agreement with experiment for both the spectral shape and the ratio of the ZPL intensity to that of the sideband (Figure 4). For the sideband intensity at the position of the LP peak, the calculated sideband/ZPL intensity ratio for $\alpha = 1$ is ~0.20, in agreement with experiment, whereas for $\alpha = 0.25$ this ratio is only ~0.012.

The insets of Figures 4 and 5 compare, for variable and constant effective mass, respectively, the shapes and relative intensities of the PH and phonon response functions used in the calculation for $\alpha = 1$. The PH response function is a factor of 5 smaller than shown in the insets, indicating in both cases that at a given (not too low) energy the glyoxal electronic transition has a stronger coupling to the collective excitations than to single PH excitations, which is consistent with what is to be expected for an interacting FL with a mass renormalization factor as large as 2.8 at the Fermi level. However, for $\mathcal{E} \to 0$ the decay of $\varphi_{PH}(\mathcal{E})$ is much slower than that of $\varphi_{phon}(\mathcal{E})$, which not only removes the pseudogap in the spectral function but also yields integrated properties (e.g., HR factors) that are comparable in size. The total HR exponent (eq 27) is $S = 3.24$, of which $S_{PH} = 2.42$ comes from PH excitations and only $S_{phon} = 0.82$ comes from phonons. Two interesting comparisons are in order: (i) in ref 13, a smooth fit of the sideband tail for glyoxal in ^{3}He was obtained with *only* PH excitations and $S = 2.50$, in good agreement with the present results; (ii) for glyoxal in ^{4}He,[5] where only collective excitations (phonons and rotons) are involved, the sideband is separated from the ZPL by the rotonic pseudogap and can be best fitted with $S = 1.61$, which is about twice as large as S_{phon} for glyoxal in ^{3}He. The larger value of the collective HR factor for ^{4}He can be explained by the presence of the roton branch, which is overdamped in ^{3}He.

The weak-coupling value $\alpha = 0.25$, corresponding to an HR exponent of $S = 0.81$, was chosen for a previous comparison with calculations of the ZPL line shape including only PH excitations.[11] In that case, $\alpha = 0.25$ provided the best fit of the ZPL line shape, but the agreement with the sideband shape where collective excitations are dominant was not as good. The inclusion of collective phonon excitations has little effect on the sharp ZPL because the response function of collective phonon excitations decays rapidly for $\mathcal{E} \to 0$, consistent with the pseudogap between the ZPL and the multiphonon sideband. The convolution with PH excitations removes the pseudogap but preserves a comparatively sharp ZPL. This result may provide an a posteriori justification of the simple addition of a ZPL to the multiple PH excitation spectrum as in the calculations of ref 10, although the convolution of the PH and collective response functions implied by eq 26 is far from being a simple sum of the two contributions. The reduction of the coupling strength, besides producing a strong depression of the sideband with respect to the ZPL, removes the long tail at

dx.doi.org/10.1021/jp503184d | J. Phys. Chem. A XXXX, XXX, XXX–XXX

high energy while making the phonon features more pronounced.

The calculations with a constant effective mass (Figure 5), also with the ZPL maximum set at a relative experimental depletion of 17%, show similar effects, although there is a much faster decay of the sideband tail because of the larger inertia of the ^{3}He q-particles in their excitations to high-energy states. This effect is even more pronounced for the collective phonon excitations, to the extent that for $\alpha = 1$ the LP and maxon features are barely visible. However, the latter become more pronounced in the weak-coupling case ($\alpha = 0.25$), as found in the variable effective mass calculations. It is clear, however, that the variable effective mass is an essential ingredient in the theory in order to explain the multiexcitation sideband and to learn something about the local dynamics of the FL. This is due to the fact that the inelastic part of the spectrum extends to energies at which the motion of the ^{3}He atoms approaches that of the bare atom with a vanishing mass renormalization.

5. DISCUSSION

The existence of Fermi liquid particle−hole excitations in ^{3}He leads to an essential difference of the zero-phonon line shape in the optical spectra of a chromophore molecule embedded inside a ^{3}He droplet in comparison with the analogous spectra in ^{4}He droplets. These excitations of the Fermi liquid are characterized by a large density of states in the low-energy limit, yielding for $\mathcal{E} \rightarrow 0$ a linear behavior of $\varphi_{\mathrm{PH}}(\mathcal{E})$ compared with a higher-power law for $\varphi_{\mathrm{phon}}(\mathcal{E})$. Unlike superfluid ^{4}He droplets,[3,5] where the sideband of collective phonon excitations is clearly separated from the ZPL by a roton pseudogap, in Fermionic ^{3}He droplets the quasi-continuum of single PH excitations completely removes the pseudogap. There is therefore a full superposition of the PH and collective excitation spectra, and their mutual convolution needs to be considered in order to quantitatively account for the structure of the experimental sideband. In view of such entanglement, the observation of a sharp phonon resonance popping out atop the dense PH continuum with a width an order of magnitude narrower than that of bulk phonons at the same energy is surprising. Two facts are now shown to play an essential role: (i) the shell structure of the Fermi liquid surrounding the doping molecule, which has a considerably larger density in the first atomic shell and a larger Fermi wavevector, and (ii) the energy dependence of the ^{3}He effective mass, which shows a large peak at the Fermi level and a kink associated with the maximum of the collective excitation energy (maxon). In effect, the dense liquid shell around the molecule acts as a quantum Helmholz resonator. There is another important statistics-related difference between the collective-excitation sideband of the glyoxal transition in ^{3}He and that in ^{4}He. Although the superfluid ^{4}He droplet has a shell structure around the glyoxal molecule with large density oscillations similar to those in ^{3}He,[25] the sideband could be reproduced using the bulk phonon/roton dispersion with only a modest softening of the roton and a small stiffening of the maxon,[5] and no localized phonon was found nor needed. On the contrary, in the ^{3}He droplet the first-shell phonon structure is dramatically modified with respect to the bulk. One possible reason for such a difference is that in ^{3}He droplets the Fermionic atoms have to distribute themselves pairwise on different states of shorter and shorter wavelengths as the energy increases; this favors localization of collective excitations, as these involve atoms near the Fermi level. In contrast, in ^{4}He the bosonic atoms are mostly in the ground state, which favors unlocalized, substantially unperturbed collective excitations.

Since the collective phonon excitations directly originate from the poles in the complex plane of the PH response function for the *interacting* Fermi liquid, and this intrinsically contains the perturbing effects of the shell formation, the global response function as well as the phase shift θ would be natural outputs of an ab initio treatment of the ^{3}He droplet dynamics along the lines traced out by Barranco and co-workers.[25,26] This aspect is beyond the scope of the present study, whose main aim was to show, by means of the powerful Lax formalism, the combined roles of single particle−hole and collective phonon excitations in determining the special shape of the ZPL sideband observed in the vibronic absorption spectrum of molecules embedded in Fermionic ^{3}He droplets. Another aim of the present analysis was to further illustrate the wealth of information about the excitation spectra of a *perturbed Fermi liquid* that can be extracted from the optical spectroscopy of probe chromophores.

AUTHOR INFORMATION

Corresponding Author

*E-mail: jtoenni@gwdg.de.

Notes

The authors declare no competing financial interest.

ACKNOWLEDGMENTS

G.B. acknowledges support from the Alexander von Humboldt (AvH) Stiftung and the Ikerbasque Foundation (Project ABSIDES). The authors acknowledge useful discussions with Prof. Pedro M. Echenique during their visits at DIPC in Donostia/San Sebastian. The research was also supported by Estonian Research Projects SF0180013s07 and IUT2-27 and by the European Union through the European Regional Development Fund (Project 3.2.0101.11-0029).

REFERENCES

(1) Toennies, J. P.; Vilesov, A. F. Superfluid helium droplets: A uniquely cold nanomatrix for molecules and molecular complexes. *Angew. Chem., Int. Ed.* **2004**, *43* (20), 2622−2648.

(2) Stienkemeier, F.; Vilesov, A. F. Electronic spectroscopy in He droplets. *J. Chem. Phys.* **2001**, *115* (22), 10119−10137.

(3) Choi, M. Y.; Douberly, G. E.; Falconer, T. M.; Lewis, W. K.; Lindsay, C. M.; Merritt, J. M.; Stiles, P. L.; Miller, R. E. Infrared spectroscopy of helium nanodroplets: Novel methods for physics and chemistry. *Int. Rev. Phys. Chem.* **2006**, *25* (1−2), 15−75.

(4) Szalewicz, K. Interplay between theory and experiment in investigations of molecules embedded in superfluid helium nanodroplets. *Int. Rev. Phys. Chem.* **2008**, *27* (2), 273−316.

(5) Hartmann, M.; Mielke, F.; Toennies, J. P.; Vilesov, A. F.; Benedek, G. Direct spectroscopic observation of elementary excitations in superfluid He droplets. *Phys. Rev. Lett.* **1996**, *76* (24), 4560−4563.

(6) Stienkemeier, F.; Ernst, W. E.; Higgins, J.; Scoles, G. On the Use of Liquid-Helium Cluster Beams for the Preparation and Spectroscopy of the Triplet-States of Alkali Dimers and Other Weakly-Bound Complexes. *J. Chem. Phys.* **1995**, *102* (1), 615−617.

(7) Stienkemeier, F.; Higgins, J.; Ernst, W. E.; Scoles, G. Laser Spectroscopy of Alkali-Doped Helium Clusters. *Phys. Rev. Lett.* **1995**, *74* (18), 3592−3595.

(8) Grebenev, S.; Toennies, J. P.; Vilesov, A. F. Superfluidity within a small helium-4 cluster: The microscopic Andronikashvili experiment. *Science* **1998**, *279* (5359), 2083−2086.

(9) Cowley, R. A.; Woods, A. D. B. Inelastic Scattering of Thermal Neutrons from Liquid Helium. *Can. J. Phys.* **1971**, *49* (2), 177−200.
(10) Poertner, N.; Toennies, J. P.; Vilesov, A. F.; Benedek, G.; Hizhnyakov, V. Anomalously sharp phonon excitations in ^{3}He droplets. *EPL* **2009**, *88* (2), No. 26007.
(11) Benedek, G.; Hizhnyakov, V. Fermi sea excitations in the optical spectrum of a doped ^{3}He droplet. *Chem. Phys. Lett.* **2012**, *548*, 17−22.
(12) Skold, K.; Pelizzari, C. A. Elementary Excitations in Liquid-He-3. *Philos. Trans. R. Soc., B* **1980**, *290* (1043), 605−616.
(13) Fåk, B.; Guckelsberger, K.; Scherm, R.; Stunault, A. Spin Fluctuations and Zero-Sound in Normal Liquid ^{3}He Studied by Neutron Scattering. *J. Low Temp. Phys.* **1994**, *97* (5−6), 445−487.
(14) Albergamo, F.; Verbeni, R.; Huotari, S.; Vanko, G.; Monaco, G. Zero sound mode in normal liquid ^{3}He. *Phys. Rev. Lett.* **2007**, *99* (20), No. 205301.
(15) Lax, M. The Franck−Condon Principle and Its Application to Crystals. *J. Chem. Phys.* **1952**, *20* (11), 1752−1760.
(16) Pines, D.; Nozieres, P. *The Theory of Quantum Liquids*; Addison Wesley: Reading, MA 1989; Vol. *I*, p 72, eq 7.2.
(17) Rebane, K. K. *Impurity Spectra of Solids: Elementary Theory of Vibrational Structure*; Plenum Press: New York, 1970.
(18) Fetter, A. L.; Walecka, J. D. *Quantum Theory of Many-Partcle Systems*; Dover: Mineola, NY, 2003.
(19) For a spherical box, the eigenvalues are $E_{nl} = u_{l,n}{}^2h^2/(8\pi^2m^*R^2)$, where $u_{l,n}$ is the nth zero of the lth spherical Bessel function and R is the droplet radius. The separations between the levels with the lowest angular and radial quantum numbers are $E_{11} - E_{10} \approx 0.342V^{-2/3}h^2/m^*$ and $E_{20} - E_{10} \approx 0.974V^{-2/3}h^2/m^*$, respectively.
(20) Friman, B. L.; Krotscheck, E. Zero Sound, Spin Fluctuations, and Effective Mass in Liquid ^{3}He. *Phys. Rev. Lett.* **1982**, *49* (23), 1705−1708.
(21) Fåk, B.; Glyde, H. R. Density and spin-density excitations in normal-liquid ^{3}He. *Phys. Rev. B* **1997**, *55* (9), 5651−5654.
(22) Glyde, H. R.; Fåk, B.; van Dijk, N. H.; Godfrin, H.; Guckelsberger, K.; Scherm, R. Effective mass, spin fluctuations, and zero sound in liquid ^{3}He. *Phys. Rev. B* **2000**, *61* (2), 1421−1432.
(23) Krotscheck, E.; Springer, J. Physical mechanisms for effective mass enhancement in He-3. *J. Low Temp. Phys.* **2003**, *132* (5−6), 281−295.
(24) The function $m^*(k)$ calculated by Krotscheck and Springer (ref 23) and by Fåk and Glyde (ref 21) has been fitted for the present analysis by $m^*(k) = 1.1 + 0.064/[(1 - k/k_F)^2 + 0.04] + (0.15)(2.5 - k/k_F)/[(2.5 - k/k_F)^2 + 0.01]$ and is plotted in Figure 2a.
(25) Barranco, M.; Guardiola, R.; Hernandez, S.; Mayol, R.; Navarro, J.; Pi, M. Helium nanodroplets: An overview. *J. Low Temp. Phys.* **2006**, *142* (1−2), 1−81.
(26) Garcias, F.; Serra, L.; Casas, M.; Barranco, M. Ground-state properties of doped ^{3}He clusters. *J. Chem. Phys.* **1998**, *108* (21), 9102−9106.
(27) Zhao, J.; Zhang, R. Proton transfer reaction rate constants betweeen hydronium ion (H_3O^+) and volatile organic compounds. *Atmos. Environ.* **2004**, *38* (14), 2177−2185.
(28) El-Kader, M. S. A.; Bancewicz, T. Dipole−octopole polarizability of sulfur hexafluoride from isotropic and anisotropic light scattering experiments. *Chem. Phys. Lett.* **2013**, *571*, 16−22.
(29) Poertner, N. Hochauflösende elektronische Spektroskopie von Molekülen in ^{4}He- und ^{3}He-Tröpfchen. Dissertation, University of Göttingen, Göttingen, Germany, 2000; Max Planck Institut für Strömungsforschung Report 1/2001.
(30) Pack, R. T.; Piper, E.; Pfeffer, G. A.; Toennies, J. P. Multiproperty Empirical Anisotropic Intermolecular Potentials. II. $HeSF_6$ and $NeSF_6$. *J. Chem. Phys.* **1984**, *80* (10), 4940−4950.
(31) Greywall, D. S. Specific-Heat of Normal Liquid-^{3}He. *Phys. Rev. B* **1983**, *27* (5), 2747−2766.
(32) Boronat, J.; Casulleras, J.; Grau, V.; Krotscheck, E.; Springer, J. Effective mass of two-dimensional ^{3}He. *Phys. Rev. Lett.* **2003**, *91* (8), No. 085302.
(33) Jortner, J.; Benhorin, N. Spectroscopic Cluster-Size Effects. *J. Chem. Phys.* **1993**, *98* (12), 9346−9351.
(34) Sartakov, B. G.; Toennies, J. P.; Vilesov, A. F. Infrared spectroscopy of carbonyl sulfide inside a pure ^{3}He droplet. *J. Chem. Phys.* **2012**, *136* (13), No. 134316.
(35) Mateo, D.; Pi, M.; Navarro, J.; Toennies, J. P. A density functional study of the structure of small OCS@^3He_N clusters. *J. Chem. Phys.* **2013**, *138* (4), No. 044321.
(36) Consider a transition from a state below the Fermi level ($k_i < k_F$) to a state above the Fermi level ($k_f > k_F$). The transition energy is $\mathcal{E} = E_f - E_i = \int_{ki}^{ki+Q} dk\, k/m^*(k)$. For $Q \to 0$, $m^*(k) \to m_F^*$, while for $Q \to \infty$, most of the integration path is for $m^*(k) \approx m_0$. Therefore, $\mathcal{E} \approx k_FQ/m_F^*$ for $Q \ll k_F$ and $\mathcal{E} \approx Q^2/2m$ for $Q \gg k_F$.
(37) Bransden, B. H.; Joachain, C. J. *Introduction to Quantum Mechanics*; Longman: New York, 1992.
(38) This is easily seen by assuming an excitation spectrum with a single frequency, $\varphi(\mathcal{E}) = \alpha\delta(\mathcal{E} - \varepsilon_0)$ and substituting this expression into eq 14 and then eq 14 into eq 12. When for simplicity δ is set equal to 0 and $F(t)$ is expanded, the Fourier transform provides the well-known Poisson series of one-, two-, ... excitation processes:

$$I(\mathcal{E}) \equiv \int dt\; e^{-i\mathcal{E}t}F(t) = e^{-S}\left[\delta(\mathcal{E}) + \frac{\alpha}{\varepsilon_0}\delta(\mathcal{E}-\varepsilon_0) + \frac{1}{2!}\left(\frac{\alpha}{\varepsilon_0}\right)^2\delta(\mathcal{E} - 2\varepsilon_0) + ...\right]$$

(39) Benedek, G.; Nardelli, G. F. Lattice Response Functions of Imperfect Crystals—Effects Due to a Local Change of Mass and Short-Range Interaction. *Phys. Rev.* **1967**, *155* (3), 1004−1019.
(40) Pryce, M. H. L. *Phonons in Perfect Lattices and in Lattices with Point Imperfections*; Oliver and Boyd: London, 1966.
(41) Gough, C. Musical Acoustics. In *Springer Handbook of Acoustics*; Rossing, T. D., Ed.; Springer Science & Business Media: New York, 2007; pp 533−668.